J Biol Inorg Chem (2008) 13:765–770
DOI 10.1007/s00775-008-0362-y

ORIGINAL PAPER

Iron–sulfur repair YtfE protein from *Escherichia coli*: structural characterization of the di-iron center

Smilja Todorovic · Marta C. Justino · Gerd Wellenreuther · Peter Hildebrandt · Daniel H. Murgida · Wolfram Meyer-Klaucke · Lígia M. Saraiva

Received: 29 November 2007 / Accepted: 7 March 2008 / Published online: 21 March 2008

Abstract YtfE was recently shown to be a newly discovered protein required for the recovery of the activity of iron–sulfur-containing enzymes damaged by oxidative and nitrosative stress conditions. The *Escherichia coli* YtfE purified protein is a dimer with two iron atoms per monomer and the type and properties of the iron center were investigated by using a combination of resonance Raman and extended X-ray absorption fine structure spectroscopies. The results demonstrate that YtfE contains a non-heme dinuclear iron center having μ-oxo and μ-carboxylate bridging ligands and six histidine residues coordinating the iron ions. This is the first example of a protein from this important class of di-iron proteins to be shown to be involved in the repair of iron–sulfur centers.

Keywords Di-iron proteins · Iron–sulfur repair · Raman spectroscopy · Extended X-ray absorption fine structure spectroscopy

Smilja Todorovic and Marta C. Justino contributed equally to this work.

Electronic supplementary material The online version of this article (doi:10.1007/s00775-008-0362-y) contains supplementary material, which is available to authorized users.

S. Todorovic · M. C. Justino · L. M. Saraiva (✉)
Instituto de Tecnologia Química e Biológica,
Universidade Nova de Lisboa,
Av. da República (EAN),
2780-157 Oeiras, Portugal
e-mail: lst@itqb.unl.pt

G. Wellenreuther · W. Meyer-Klaucke
EMBL Outstation c/o DESY,
Notkestrasse 85,
22603 Hamburg, Germany

P. Hildebrandt · D. H. Murgida
Sekr. PC 14, Max-Volmer-Laboratorium
für Biophysikalische Chemie,
Institut für Chemie,
Technische Universität Berlin,
Straße des 17. Juni 135,
10623 Berlin, Germany

Introduction

Proteins that contain iron–sulfur clusters are the most ubiquitous metalloproteins in nature, performing a wide range of biological processes that are essential to the metabolism of the cell [1–3]. However, these clusters are rapidly damaged under oxidative and nitrosative stress conditions, generating inactive proteins. Nature has developed systems that specifically promote repair, and the YtfE of *Escherichia coli* is the most recently discovered system involved in the repair of degraded iron–sulfur clusters [4]. Deletion of *ytfE* significantly alters the phenotype of *E. coli*, generating a strain with enhanced susceptibility to nitrosative stress and defective in the activity of several iron–sulfur-containing proteins [5, 6]. Furthermore, in the absence of *ytfE* the damage to enzymes containing iron–sulfur clusters caused by exposure to hydrogen peroxide or nitric oxide stress occurs at higher rates, and recovery of the activity is only attained upon addition of purified holo-YtfE [4].

Homologues of YtfE can be found in a large number of organisms, including bacteria, parasites and higher eukaryotes. Analysis of the amino acid sequence of these proteins reveals the presence of conserved carboxylate (aspartate and glutamate) and histidine residues that could constitute the ligands for a dinuclear non-heme iron center [6]. In fact, studies on *E. coli* YtfE by electron paramagnetic

resonance spectroscopy suggested that it contains a di-iron site [5]. However, *E. coli* YtfE does not share a significant degree of sequence similarity with the known di-iron proteins, neither is the proposed function related to the di-iron enzymes described so far [7]. In this work we present the detailed structural characterization of *E. coli* YtfE's active site, carried out using resonance Raman and extended X-ray absorption fine structure (EXAFS) spectroscopies, which allowed the design of a structural model for the di-iron center of YtfE.

Materials and methods

Production of the *E. coli* recombinant YtfE protein

The recombinant YtfE protein was produced in *E. coli* Bl21Gold(DE3) cells (Stratagene) freshly transformed with the plasmid pET-YtfE [5], grown aerobically at 30 °C in M9 minimal medium [8] with 20 mM glucose, 100 μM $FeSO_4$ and 30 μg mL^{-1} kanamycin, in a 10-L fermentor. When the cultures reached an optical density at 600 nm of 0.3, 400 μM isopropyl-1-thio-β-D-galactopyranoside was added and after 6 h the cells were harvested by centrifugation. The cells were disrupted in a French press and the protein was purified as previously described [5]. The protein concentration was assayed by the bicinchoninic acid method [9], and the iron content was determined by the 2,4,6-tripyridyl-1,2,3-triazine method [10]. The purified protein contained two iron atoms per monomer.

Resonance Raman analysis

About 2 μL of 1.5 mM oxidized *E. coli* YtfE [20 mM Tris-HCl, pH 7.5, 150 mM NaCl] was introduced into a liquid-nitrogen-cooled cryostat (Linkam) mounted on a microscope stage and cooled down to 77 K. Spectra from the frozen sample were collected in backscattering geometry by using a confocal Raman microscope (Jobin Yvon, XY), with the 413-nm excitation line from a krypton ion laser (Coherent Innova 302). For isotopic labeling, oxidized protein was lyophilized and then brought up in $H_2{}^{18}O$, and $D_2{}^{16}O$, and then measured as described above.

Typically, spectra were accumulated for 60 s with a laser power at sample of 8 mW. After polynomial background subtraction, the positions of the Raman bands were determined for each sample.

Preparation of samples for EXAFS analysis

All samples contained the YtfE protein at 0.5 mM in 20 mM Tris-HCl pH 7.5. The sample of oxidized YtfE was prepared by addition of a 50 mM solution of potassium persulfate, in a twofold molar excess. The sample was introduced into the cuvette through a capillary, using argon flux to push the transfer, and was immediately frozen in liquid nitrogen. The reduced and NO-treated samples were prepared anaerobically under a continuous argon flux. The protein solutions were first made anaerobic by flushing them with argon for 10 min, and were then treated and transferred to appropriate cuvettes as described above. To prepare the reduced sample, an anaerobic solution of 50 mM sodium dithionite was added in a twofold molar excess. Treatment with nitric oxide was done in a 1:1 ratio of nitric oxide to iron, by addition of 25 μL of nitric oxide water-saturated solution (2 mM) [6] to 25 μL of anaerobic YtfE protein (1 mM).

X-ray absorption spectroscopy measurements

The iron K-edge X-ray absorption spectra were recorded at beamline D2 of the EMBL Outstation Hamburg at DESY, Germany. The DORIS storage ring was operated at 4.5 GeV with the positron beam current ranging from 145 to 80 mA. A Si(111) double-crystal monochromator scanned X-ray energies around the iron K-edge (6.9–7.7 keV). Harmonic rejection was achieved by a focusing mirror (cutoff energy at 20.5 keV) and a monochromator detuning to 50% of its peak intensity. The sample cells were mounted in a two-stage Displex cryostat and kept at about 20 K. The X-ray absorption spectra were recorded as iron K_α fluorescence spectra with a Canberra 13-element Ge solid-state detector. The detector is frozen (dead time) while a pulse is being processed. We ensured that no more than 20% of the counts occurred in this period and corrected each data point for this effect. For each sample a different number of scans was performed and the results were averaged to ensure comparable statistics. X-ray energy calibration was achieved by recording Bragg reflections from a static Si(220) crystal in back-reflection geometry during each scan [11]. Data reduction, such as background removal, normalization and extraction of the fine structure, was performed with KEMP [12] assuming a threshold energy $E_{0,Fe}$ of 7,120 eV.

X-ray absorption near-edge structure analysis

The intensities and energies of the $1s \rightarrow 3d$ pre-edge features of the normalized iron K-edge absorption spectra were quantified using the program WinXAS [13]. The spectra were fitted over 13 eV around the pre-edge features and modeled by pseudo-Voigt peak shapes. The energy position, the full width at half maximum and the peak height were refined. The background underneath the pre-edge features was modeled as well by a pseudo-Voigt function. The total intensity of the $1s \rightarrow 3d$ pre-edge

feature was assigned to the area of the pseudo-Voigt peak at about 7,113 eV.

EXAFS analysis

The extracted iron K-edge (15–570 or 15–520 eV) EXAFS data were converted to photoelectron wave vector k-space and weighted by k^3. The spectra were initially analyzed by ABRA [14] and afterwards refined with EXCURV98 [15]. The program calculated the theoretical EXAFS for defined structural models based on the curved-wave theory. In addition to single scattering contributions multiple scattering linear units were defined for Fe–His and Fe–N–O. Parameters of each structural model, namely, the atomic distances (R), the Debye–Waller factors ($2\sigma^2$) and a residual shift of the energy origin (Fermi energy) were refined, minimizing the fit index (Φ) by applying restraints for the predefined units [15]. An amplitude reduction factor of 1.0 was used throughout the data analysis.

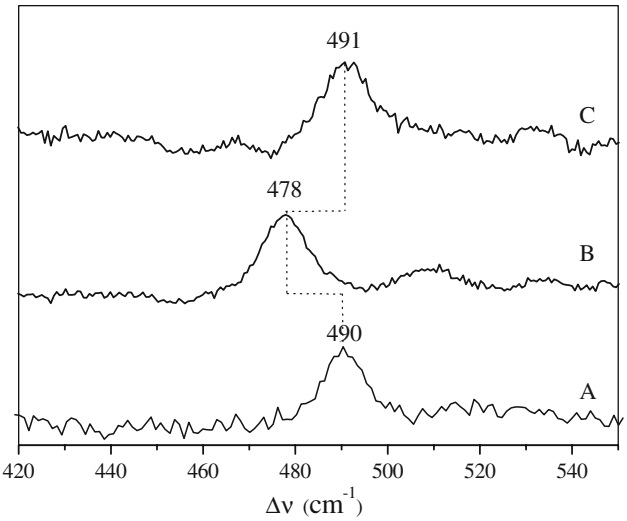

Fig. 1 Resonance Raman spectra of *A* 1.5 mM oxidized *Escherichia coli* YtfE in $H_2{}^{16}O$/Tris-HCl, pH 7.5; isotopically labeled with *B* $H_2{}^{18}O$ and *C* $D_2{}^{16}O$. The spectra were obtained at 77 K with 413-nm excitation, a laser power of 8 mW and 60-s accumulation time

Results

Resonance Raman spectroscopy of *E. coli* YtfE

Resonance Raman spectroscopy is a powerful tool for studying non-heme iron proteins. Upon excitation in resonance with a ligand-to-metal charge transfer transition, modes involving the metal–ligand stretching coordinates are selectively enhanced, thus allowing one to draw conclusions about the nature of the ligands and the coordination geometry of the complex.

In the oxidized state of YtfE the ligand-to-iron charge transfer transition gives rise to a weak absorption band at 350 nm. Thus, the 413-nm excitation line can be employed to provide a resonance enhancement of the iron–ligand stretching modes which are expected in the low-frequency region below 600 cm^{-1}. The resonance Raman spectrum of YtfE in $H_2{}^{16}O$ displays one band at 490 cm^{-1} (Fig. 1, spectrum A), which lies in the range of symmetric Fe–O–Fe stretching modes (ν_s) of μ-oxo-bridged di-iron centers in proteins and model complexes [16, 17]. On the basis of empirical relationships previously derived for model compounds [18], the ν_s frequency is characteristic of dibridged complexes containing one μ-oxo and one μ-carboxylate ligand; however, it also falls in the range observed for protein-bound μ-oxo-bridged di-iron centers which involve two μ-carboxylate ligands. Both assignments are consistent with the results of isotopic labeling. In these experiments, the protein was lyophilized and then redissolved in $H_2{}^{18}O$ to substitute the bridging oxygen by ^{18}O [17–19]. The UV–vis absorption spectrum confirmed that the di-iron core remained intact upon removal and subsequent addition of water (data not shown). As a consequence of the isotopic substitution, the 490-cm^{-1} band undergoes a downshift by approximately 12–478 cm^{-1} (Fig. 1, spectrum B). Also the $^{18}O/^{16}O$ shift of the ν_s mode is characteristic of μ-oxo-bridged di-iron centers either with one or with two additional carboxylate bridges [17, 18, 20]. No spectral changes were observed when the protein was dissolved in D_2O, ruling out the involvement of a bridging hydroxyl ligand (Fig. 1, spectrum C).

EXAFS analysis of the *E. coli* YtfE

Oxidized and reduced forms of YtfE and the as-prepared enzyme incubated with NO were analyzed by iron K-edge X-ray absorption spectroscopy. Two parts of the spectrum were analyzed independently. The edge region (X-ray absorption near-edge structure, XANES), in particular the intensity of the $1s \rightarrow 3d$ transition (pre-edge peak), is sensitive to the electronic and geometric structure of the iron site and serves as an indicator for the coordination number and/or ligand sphere homogeneity. Details on the type of ligands and their metal distances were extracted from the fine structure (EXAFS).

The XANES pattern of oxidized YtfE (Fig. 2) exhibits a double-peak structure of the rising edge at approximately 7,130 eV accompanied by an intense pre-edge peak at approximately 7,113 eV. The pre-edge peak intensity of about 20×10^{-2} eV indicates the absence of a perfect octahedral coordination. The incubation of the enzyme with NO resulted in a similar spectrum. The slightly lower intensity and the 20% increase in the pre-edge peak intensity can originate either from a lower coordination

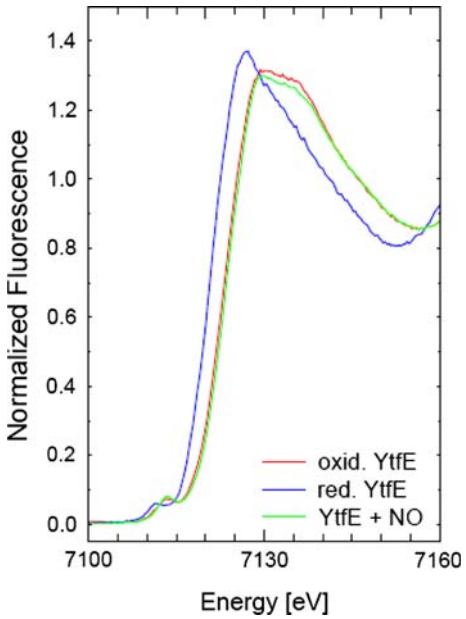

Fig. 2 X-ray absorption near-edge structure spectra for YtfE in the oxidized (*oxid. YtfE*) and the reduced (*red. YtfE*) state and for the as-prepared protein incubated with NO (*YtfE + NO*). The distinct shift in the edge position, defined as half of the normalized edge jump, by more than 2 eV between reduced and oxidized enzyme visualizes the change in the iron oxidation state from Fe(II) to Fe(III) for both metal ions. Incubation of NO does not affect the metal oxidation state

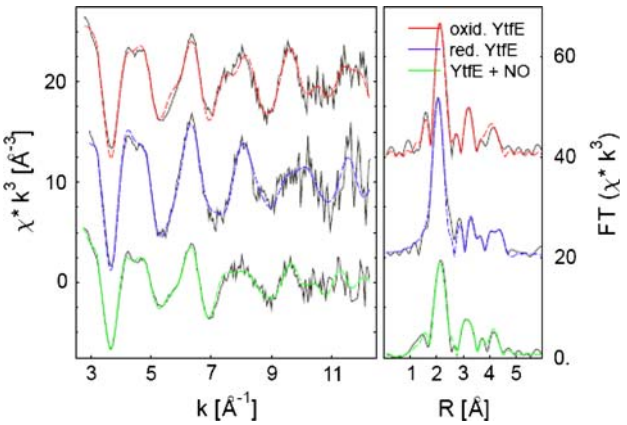

Fig. 3 Extracted extended X-ray absorption fine structure (EXAFS) spectra and corresponding Fourier transforms for YtfE in the oxidized (*oxid. YtfE*) and the reduced (*red. YtfE*) state and for the as-prepared protein incubated with NO (*YtfE + NO*). All three EXAFS spectra exhibit a camel-back feature at about 4.5 Å^{-1} indicative of the presence of imidazole ligands. This is consistent with the contribution at about 4 Å in the Fourier transform, enhanced by the multiple scattering within this unit

number or from a more inhomogeneous ligand sphere. This question is addressed in the EXAFS analysis. The XANES of reduced YtfE shows no similarity with that for two other spectra. The shift in the edge position by 2 eV towards lower energies reflects the change from ferric to ferrous iron. The higher white line intensity at 7,122 eV points towards a more homogenous ligand sphere in this redox state (Fig. 2).

The EXAFS spectra of YtfE provide further insight into the metal coordination (Fig. 3). The spectra are dominated by a single oscillation frequency, which indicates the presence of only light ligands, such as oxygen and nitrogen. At the same time, the EXAFS amplitude for oxidized YtfE and NO-treated YtfE is relatively small, which could indicate the presence of ligands with considerably different bond lengths. These considerations define the dinuclear structural models that were compared with the data. In line with the rather high pre-edge peak intensity, the EXAFS analysis for oxidized YtfE models with small coordination numbers as well as models with a single short μ-oxo bridge were compared with the data (Table S1). A total coordination number of 6 with one short oxo group at 1.82 ± 0.01 Å, three imidazole groups and two oxygens at 2.10 ± 0.01 Å gave by far the best fit to the data. The iron–iron distance was refined to 3.54 ± 0.03 Å. In fact, the majority of the first-shell distances are slightly longer than in other non-heme iron enzymes with mixed histidine and oxygen coordination [21]. This is in line with the presence of a single ligand at shorter distances, as indicated by bond valence sum analysis [22]. The bond lengths coincide with reference values [23, 24] and no additional ligands, such as sulfur, improve the fit.

The incubation of YtfE with NO alters the iron coordination as visualized by the lower EXAFS amplitude and the lower peak height of the first-shell contribution at about 2 Å in the Fourier transform (Fig. 3). Concomitantly, the width of this peak increases, indicating the presence of an additional ligand at shorter distances causing destructive interference between the individual backscattering contributions. The correspondent EXAFS refinement is consistent with the presence of three histidine and two oxygen ligands at an average distance of 2.11 ± 0.01 Å and the presence of one NO or μ-oxo bridge bound to each of the iron ions at a distance of 1.82 ± 0.02 Å. The metal–metal distance is identical to that of the oxidized YtfE within the error margins (3.50 ± 0.04 Å).

The iron coordination of the reduced YtfE differs considerably. The EXAFS amplitude is higher and the frequency lower (Fig. 3), reflecting more ligands or a higher degree of order as well as a shorter average bond length. This is revealed by the refinement results: an average bond length of 2.08 ± 0.01 Å is determined for three histidine and 2.5 oxygen ligands. The metal–metal distance refines to 3.71 ± 0.06 Å. The absence of a short μ-oxo bridge is in line with the longer metal–metal distance.

The EXAFS refinement parameters modeling best YtfE in the oxidized and reduced states and incubated with NO are shown in Table 1. Some less satisfactory alternative models compared with the data are given in Table S1.

Table 1 Extended X-ray absorption fine structure (EXAFS) refinement parameters for oxidized, reduced and NO-incubated YtfE

N	Fe···L	*R* (Å)	$2\sigma^2$ (Å^2)	Fermi energy (eV)	Φ
Oxidized YtfE, $k_{max} = 12.2$ Å^{-1}					
1	Fe···O	1.82 (1)	0.013 (2)[b]	−6.4 (6)	0.4770
2	Fe···O	2.097 (6)[a]	0.013 (2)[b]		
3	Fe···His(N)	2.097 (6)[a]	0.013 (1)[b]		
3	Fe···His(C)	3.10 (6)	0.005 (4)[c]		
3	Fe···His(C)	3.15 (3)	0.005 (4)[c]		
3	Fe···His(C)	4.31 (2)	0.003 (2)[d]		
3	Fe···His(N)	4.50 (4)	0.003 (2)[d]		
1	Fe···Fe	3.54 (3)	0.018 (7)		
Reduced YtfE, $k_{max} = 12.2$ Å^{-1}					
1	Fe···O	2.076 (8)[a]	0.014 (1)[b]	−2.7 (8)	0.7136
3	Fe···His(N)	2.076 (8)[a]	0.014 (1)[b]		
3	Fe···His(C)	2.94 (3)	0.003 (3)[c]		
3	Fe···His(C)	3.18 (3)	0.003 (3)[c]		
3	Fe···His(C)	4.23 (4)	0.01 (1)[d]		
3	Fe···His(N)	4.42 (5)	0.01 (1)[d]		
1	Fe···Fe	3.71 (6)	0.02 (1)		
NO-incubated YtfE, $k_{max} = 12.2$ Å^{-1}					
1	Fe···O	1.82 (2)	0.021 (2)[b]	−7.0 (6)	0.5571
2	Fe···O	2.106 (9)[a]	0.021 (2)[b]		
3	Fe···His(N)	2.106 (9)[a]	0.021 (2)[b]		
3	Fe···His(C)	3.18 (4)	0.01 (1)[c]		
3	Fe···His(C)	3.30 (4)	0.01 (1)[c]		
3	Fe···His(C)	4.32 (2)	0.008 (7)[d]		
3	Fe···His(N)	4.53 (3)	0.008 (7)[d]		
1	Fe···Fe	3.50 (4)	0.023 (3)		

The average numbers (*N*) of ligand atoms (*L*), their distance to the iron ion (*R*), the respective Debye–Waller factor ($2\sigma^2$), the Fermi energy for all shells, and the fit index (Φ), indicating the quality of the fit are shown. For the NO group and the Fe–His units multiple scattering has been included. Values in *parentheses* represent statistical errors (2 times the standard deviation) of the least-squares refinement. The total error is estimated to 0.02–0.03 Å for first-shell distances and 0.05–0.1 Å for the other more remote backscatterers. The coordination number in EXAFS data analysis has a typical error of about 20%. In order to lower the number of parameters in the restrained refinement, distances and Debye–Waller factors for ligands of the same coordination sphere were refined jointly as indicated by *superscripts*

Discussion

Previous studies on the recombinant *E. coli* YtfE suggested that YtfE is a di-iron-containing protein, having in its primary sequence several histidines and carboxylates that may serve as ligands to the iron atoms [6, 25]. The resonance Raman spectroscopy results indicate a μ-oxo-bridged di-iron center. The frequency of the symmetric Fe–O–Fe stretching and the $^{18}O/^{16}O$ isotopic shift are

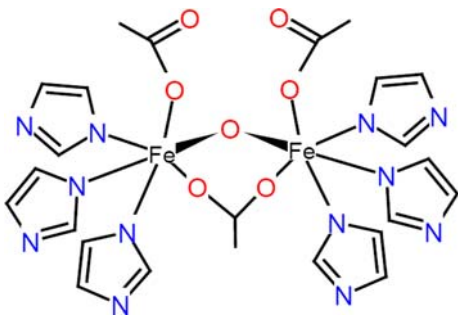

Fig. 4 Model of the *E. coli* YtfE di-iron center in the oxidized state. The two upper oxygen ligands of both iron atoms can also be provided by only one carboxylate group, thus leading to the formation of a second μ-carboxylate bridge

consistent with a complex that contains one μ-oxo and one or two μ-carboxylate bridges, the latter being provided by aspartate or glutamate residues. Further EXAFS analysis reveals an average iron coordination in the oxidized state by three imidazole groups, two oxygen ligands and a bridging μ-oxo group, which is consistent with the resonance Raman data, suggesting a structure in which both iron atoms, FeA and FeB, bind three histidine residues. These residues are as well identified in the reduced state, but the presence of the μ-oxo bridge can no longer be confirmed.

In line with the changes of the μ-oxo bridge, the Fe–Fe distance in YtfE appears to vary between the resting ferric and fully reduced (diferrous) states. In the reduced state a long metal–metal distance is determined, whereas in the oxidized state the μ-oxo group bridges the metal ions, keeping them at shorter distance. The terminal coordination geometry and ligands of both irons do change upon diferrous/diferric interconversion. For the diferrous state on average half a ligand less per iron atom is found in the refinement. Although this result is within the error margin of 20% for coordination numbers determined by EXAFS spectroscopy, this could indicate a break of the μ-oxo bridge. Taken together, the resulting small change in the major first shell ligand distances indicates a remarkable structural stability of this dinuclear site.

NO is known to form a stable complex with iron-containing proteins and thus NO may bind to either of the iron atoms. Recently it was reported that an orthologue of *E. coli* YtfE, the NorA protein of *Ralstonia eutropha*, is also capable of binding NO to its di-iron center [26]. Indeed, EXAFS spectra of YtfE incubated with NO differ from those of the oxidized form of the protein although in the refinement no significant formation of a single {FeNO} species can be identified. Binding of NO did not induce alterations either in metal–metal distance or in the type and number of iron ligands, but the replacement of the μ-oxo

group by an NO group at either of the iron ions cannot be excluded.

Figure 4 presents a structural model proposed for the *E. coli* YtfE center on the diferric state based on the spectroscopic data obtained in this work. Note that in this model the two upper oxygen ligands of the iron atoms can also be provided by only one carboxylate group, leading to the formation of a second μ-carboxylate bridge, resulting in a structure similar to that of the di-iron center of hemerythrin [16].

It is generally observed that di-iron proteins have a four-helix bundle protein fold surrounding two iron atoms which are separated by 4 Å or less. Furthermore, these metal ions have terminal carboxylate and/or histidine ligands, and a bridging oxo, hydroxo or aqua ligand at least in the ferric state [7]. *E. coli* YtfE and its homologues match all these criteria. A broad analysis of the widespread YtfE-like proteins that includes over 100 sequences shows a strict conservation of five histidine amino acid residues, and that six histidine residues are conserved in a smaller set of proteins. There is also a conservation of aspartate and glutamate residues [6, 25]. These residues are candidates for forming the binding sphere of the di-iron center. Furthermore, all YtfE-like proteins have a four-helix bundle predicted secondary structure [6, 25]. On the other hand, the YtfE di-iron center is involved in a function which has not been described so far for any other known di-iron-containing proteins, which may reflect the lack of significant overall sequence similarity between YtfE and other di-iron proteins. YtfE is an example of how subtle differences in the structure of the di-iron active site together with the surrounding polypeptide matrix modulate the chemical properties of the core and generate distinct enzyme functions. In conclusion, this work provides the structural characterization of the first di-iron protein shown to be involved in the repair of iron–sulfur proteins.

Acknowledgments Work in the laboratory of L.M.S. was funded by FCT project POCI/SAU-IMI/56088/2004 and a FCT SFRH/BD/13756/2003 studentship to M.C.J. We thank Miguel Teixeira for helpful discussions.

References

1. Beinert H, Holm RH, Munck E (1997) Science 277:653–659
2. Kiley PJ, Beinert H (2003) Curr Opin Microbiol 6:181–185
3. Johnson DC, Dean DR, Smith AD, Johnson MK (2005) Annu Rev Biochem 74:247–281
4. Justino MC, Almeida CC, Teixeira M, Saraiva LM (2007) J Biol Chem 282:10352–10359
5. Justino MC, Almeida CC, Goncalves VL, Teixeira M, Saraiva LM (2006) FEMS Microbiol Lett 257:278–284
6. Justino MC, Vicente JB, Teixeira M, Saraiva LM (2005) J Biol Chem 280:2636–2643
7. Kurtz Jr DM (1997) J Biol Inorg Chem 2:159–167
8. Sambrook J, Fritsch EF, Maniatis T (1989) Molecular cloning: a laboratory manual. Cold Spring Harbor Laboratory Press, Cold Spring Harbor
9. Smith PK, Krohn RI, Hermanson GT, Mallia AK, Gartner FH, Provenzano MD, Fujimoto EK, Goeke NM, Olson BJ, Klenk DC (1985) Anal Biochem 150:76–85
10. Fischer DS, Price DC (1964) Clin Chem 10:21–31
11. Pettifer RF, Hermes C (1985) J Appl Crystallogr 18:404–412. doi:10.1107/S0021889885010627
12. Korbas M, Marsa DF, Meyer-Klaucke W (2006) Rev Sci Instrum 77:063105-1–063105-5
13. Ressler T (1998) J Synchrotron Radiat 5:118–122. doi:10.1107/S0909049597019298
14. Wellenreuther G, Meyer-Klaucke W (2007) AIP Conf Proc 882:322–324
15. Binsted N, Strange RW, Hasnain SS (1992) Biochemistry 31:12117–12125
16. Kurtz DM (1990) Chem Rev 90:585–606
17. Fox BG, Shanklin J, Ai J, Loehr TM, Sanders-Loehr J (1994) Biochemistry 33:12776–12786
18. Sanders-Loehr J, Wheeler WD, Shiemke AK, Averill BA, Loehr TM (1989) J Am Chem Soc 111:8084–8093
19. Ravi N, Prickril BC, Kurtz DM Jr, Huynh BH (1993) Biochemistry 32:8487–8491
20. Shiemke AK, Loehr TM, Sanders-Loehr J (1986) J Am Chem Soc 108:2437–2443
21. Meyer-Klaucke W, Winkler H, Schünemann V, Trautwein AX, Nolting HF, Haavik J (1996) Eur J Biochem 241:432–439
22. Thorp HH (1998) Inorg Chem 37:5690–5692
23. Harding MM (2006) Acta Crystallogr D Biol Crystallogr 62:678–682
24. Eckert NA, Stoian S, Smith JM, Bominaar EL, Munck E, Holland PL (2005) J Am Chem Soc 127:9344–9345
25. Overton TW, Justino MC, Li Y, Baptista JM, Melo AMP, Cole JA, Saraiva LM (2008) J Bacteriol 01733–01707. doi:10.1128/jb.01733-07
26. Strube K, de Vries S, Cramm R (2007) J Biol Chem 282:20292–20300